FISEVIER

Contents lists available at ScienceDirect

Surface & Coatings Technology

journal homepage: www.elsevier.com/locate/surfcoat



The effect of electropulsing-assisted ultrasonic nanocrystal surface modification on the microstructure and properties of 300M steel



Weidong Zhao^{a,b}, Daoxin Liu^{a,*}, Xiaohua Zhang^a, Hao Zhang^b, Jun Liu^b, Chi Ma^b, Ruixia Zhang^b, Yalin Dong^b, Chang Ye^{b,*}

- ^a Corrosion and Protection Research Laboratory, Northwestern Polytechnical University, 127 You Yi Xi Road, Xi'an 710072, China
- ^b Department of Mechanical Engineering, The University of Akron, Akron, OH 44325, USA

ARTICLE INFO

Keywords:

Electropulsing-assisted ultrasonic nanocrystal surface modification Pulsed current Electroplasticity Hardness Wear resistance

ABSTRACT

In this study, electropulsing-assisted ultrasonic nanocrystal surface modification (EP-UNSM) was used to process 300M steel. It has been demonstrated that pulsed current can more effectively improve the plasticity of 300M steel as compared to continuous current having the same effective current density, even though the bulk temperature (around 150 °C) and thus the thermal effect is the same. It is believed that a pulsed current, which has a much higher peak current density, can more effectively activate pinned dislocations and can better assist the deformation-based surface modification process. EP-UNSM treatment of the steel resulted in much higher surface hardness and greater plastically affected depth as compared to both UNSM and continuous current-assisted UNSM (CC-UNSM). As a result, EP-UNSM treatment imparted much higher wear resistance to the steel than either UNSM or CC-UNSM treatment. It has been demonstrated that pulsed current can effectively improve the process effectiveness of the selected deformation-based surface engineering process (UNSM) without significantly increasing the temperature.

1. Introduction

Ultrasonic nanocrystal surface modification (UNSM) is a recently developed surface severe plastic deformation method that can significantly enhance the surface strength and wear resistance of various metals by refining grains and introducing greater surface hardness and compressive residual stress [1-4]. For example, Wu et al. [5] found that UNSM significantly increased the fatigue life of carbon steel by inducing grain refinement and compressive residual stresses. Amanov et al. [6] reported that UNSM dramatically refined surface grain size and generated a large amount of surface work hardening in a copper-based alloy, leading to a lower friction coefficient and wear rate for the alloy. It is similar to other surface severe plastic deformation processes in that the effectiveness of UNSM is remarkably dependent on the plasticity of the target material. For difficult-to-deform metals with poor plasticity. such as 300M ultra-high strength steel (300M steel), it is challenging for UNSM to induce significant changes in the microstructure and residual stresses without causing micro-cracks in the sample surface.

In recent years, pulsed electric current has been widely used to assist many deformation-based surface processing methods, including turning [7–9], ultrasonic surface rolling process (USRP) [10–12], and

laser shock peening (LSP) [13]. For example, Ji et al. [14] demonstrated that EP could assist ultrasonic peening to significantly improve the degree of grain refinement in copper. Zhang et al. [13] also reported that electropulsing-assisted laser shock peening (EP-LSP) can induce higher surface hardness and a deeper plastically affected layer in the titanium alloy Ti-6Al-4V than continuous current—assisted LSP, even though the bulk temperature for both processes is the same. The so-called non-thermal effect is responsible, at least partially, for the higher process effectiveness of EP-LSP. This non-thermal effect to the plasticity of the magnesium alloy AZ31B [15] and the titanium alloy Ti64 [13] has been demonstrated through tensile tests.

Pulsed current has also been integrated with UNSM to improve the processing effectiveness. For example, Ma et al. [16] studied electropulsing-assisted UNSM (EP-UNSM) and demonstrated that compared with EP or UNSM alone, EP-UNSM could more significantly improve the plasticity of a metallic glass by inducing more free volume and nanocrystal formation in the amorphous matrix. Ye et al. [17] also reported that EP-UNSM dramatically improves the surface finish and hardness of Ti-6Al-4 V by inducing more severe plastic deformation as compared to traditional UNSM treatment. However, neither of these studies explored the use of a pulsed current rather than a continuous current to assist

E-mail addresses: liudaox@nwpu.edu.cn (D. Liu), changye2002@gmail.com (C. Ye).

^{*} Corresponding authors.

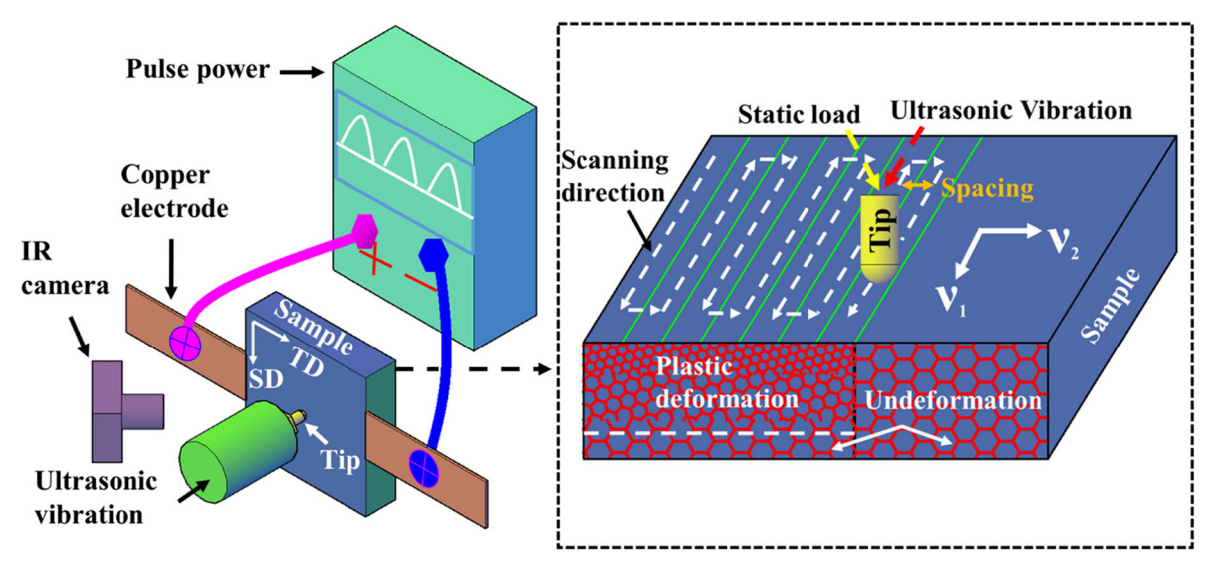


Fig. 1. Schematic representation of the EP-UNSM process.

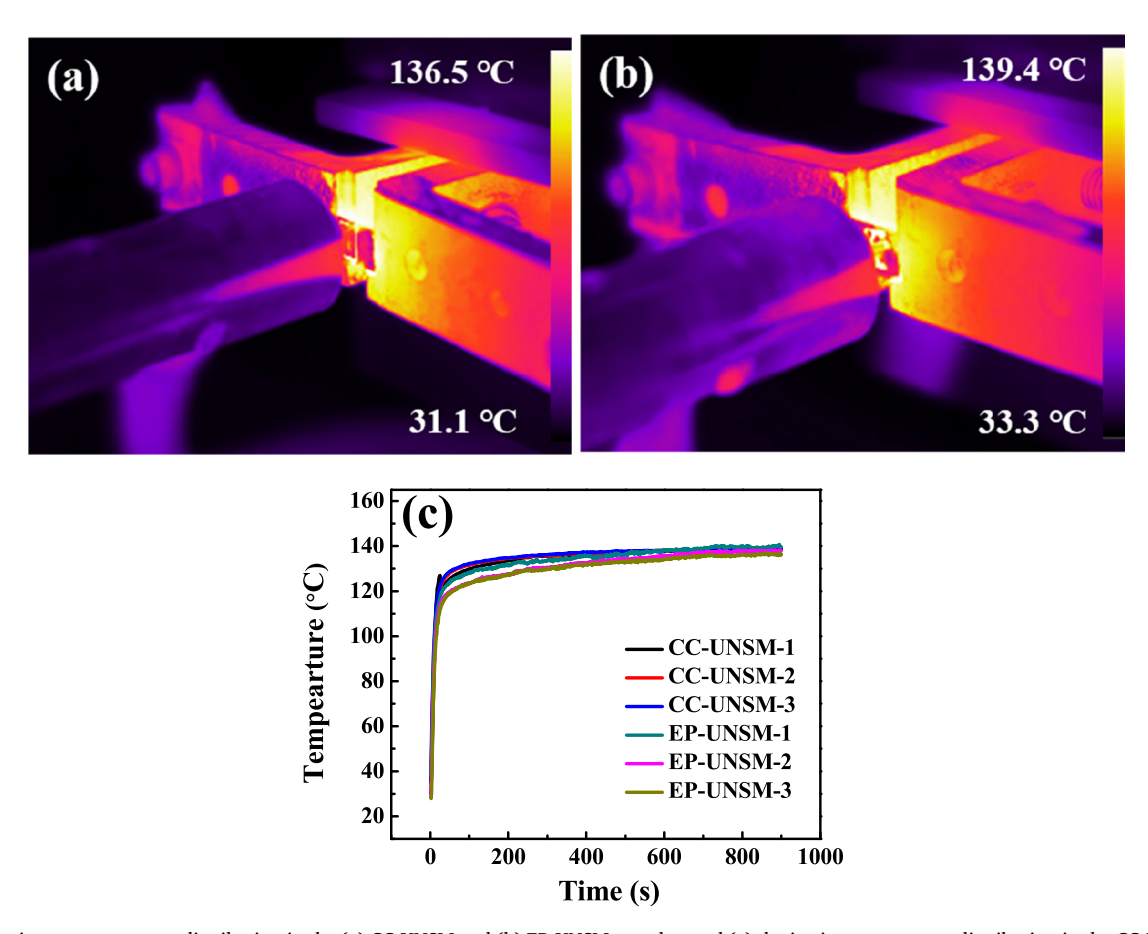


Fig. 2. The maximum temperature distribution in the (a) CC-UNSM and (b) EP-UNSM samples, and (c) the in-situ temperature distribution in the CC-UNSM and EP-UNSM samples.

UNSM. It is thus not clear if the enhanced processing effect is due entirely to the thermal effect from resistive heating.

In this study, EP-UNSM was used to process 300M steel (a hard-to-deform metal) and a comparison was made to the same steel processed using continuous current–assisted UNSM (CC-UNSM). Because the carbon atoms in martensite are easy to dissolve at high temperature, it is desirable to process the 300M steel at a relatively low temperature to ensure that the mechanical properties of the material are not affected.

Given the possibility that a pulsed current could significantly improve the plasticity of the metal with only a moderate increase in temperature, it is of interest to study the effect of EP-UNSM on 300M steel. It is expected that EP-UNSM can dramatically improve the surface hardness and wear resistance of 300M steel by inducing deeper plastic deformation in the surface layer.

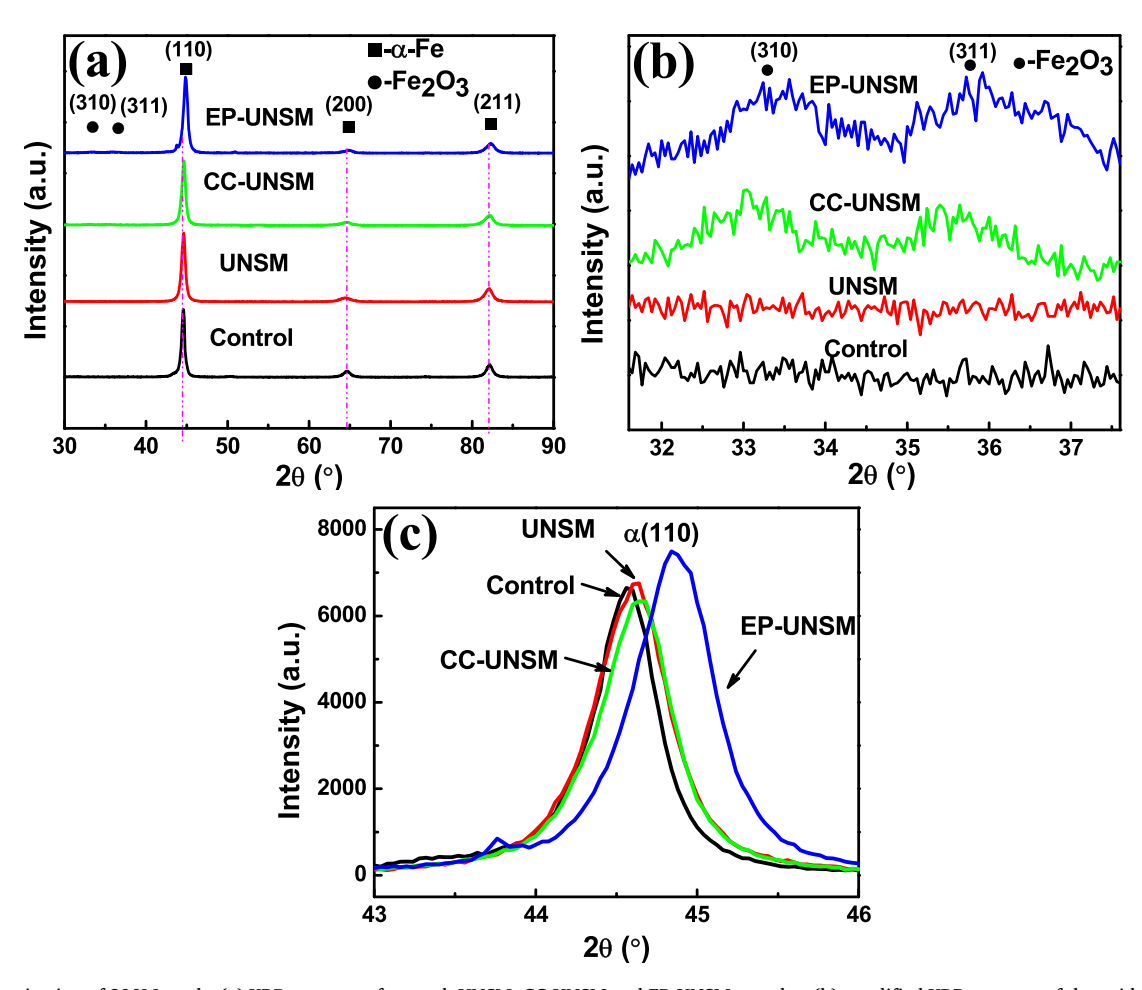


Fig. 3. Characterization of 300M steels: (a) XRD patterns of control, UNSM, CC-UNSM and EP-UNSM samples; (b) amplified XRD patterns of the oxide peaks; and (c) main α phase with (110) plane reflection.

2. Experimental program

2.1. Materials and the EP-UNSM process

The chemical composition (in wt%) of 300M steel is 0.42% carbon, 1.57% silicon, 0.82% manganese, 0.84% chromium, 1.94% nickel, 0.38% molybdenum, and 0.84% copper, with the balance in iron. The yield strength and tensile strength of the material used in this experiment can reach 1631 MPa and 2015 MPa, respectively. In this study, specimens with dimensions of 13 mm \times 10 mm \times 3 mm were mechanically polished using silicon carbide (SiC) sandpapers (320 $^{\#}$, 600 $^{\#}$, 800 $^{\#}$ and 1200 $^{\#}$) and a 1- μ m diamond suspension before treatment.

In the EP-UNSM process (Fig. 1), the sample is subjected simultaneously to UNSM treatment and a pulsed current. Before UNSM processing, a pulsed current is introduced in the sample for 100 s to obtain a stable sample temperature. The pulsed current waveform used in this study was a half sine wave with a pulse width of 100 μs . The pulsed current had a voltage of 35 V and a frequency of 250 Hz, which resulted in a peak current density in the sample of 26.45 A/mm² and a rootmean-square (RMS) current density of 2.99 A/mm². The UNSM processing was conducted using a tungsten carbide tip (with a diameter of 2.4 mm), an ultrasonic frequency of 20 kHz, a static load of 50 N, a dynamic load (amplitude) of 24 μm , a scanning speed of 250 mm/min, and a spacing between neighbor scans of 10 μm .

In order to determine if there are any other effects in addition to the thermal effect in EP-UNSM, CC-UNSM was conducted on 300M steel samples while the bulk temperature was kept constant. A FLIR T650sc infrared camera was used to measure the sample temperature. The

emissivity of the sample was calibrated by comparing the measured temperature with the temperature obtained using a Traceable Products Type K Big-Digit 4004 thermocouple. According to the calibration results, the emissivity of 300M steel was determined to be 0.33. As can be noticed in Fig. 2, the sample surface temperature was measured in situ during the CC-UNSM and EP-UNSM processes using IR camera. Each process was measured three times, which was labeled by CC-UNSM-1,2,3 and EP-UNSM-1,2,3 in Fig. 2c. The results showed that CC-UNSM with an effective current density of 3 A/mm² resulted in a temperature distribution that was similar to that in the EP-UNSM experiment. The sample surface temperature during the CC-UNSM and EP-UNSM processes remained stable in the whole process. In addition, it can be observed that neither electropulsing nor continuous current significantly increased the sample temperature (below 150 °C).

2.2. Sample characterization

2.2.1. Surface topography

Since surface topography has a significant influence on the wear properties of metals, the surface morphology of the treated and untreated 300M steel samples was measured using a Zygo NewView 7300 surface profilometer at $400\times$ magnification.

2.2.2. X-ray diffraction

A Rigaku Ultima IV X-ray diffraction (XRD) diffractometer operated at 40 kV and 35 mA was used to study the phase change in the samples processed using different treatments. A Cu-K α radiation source and a scanning speed was 1.0°/min were used.

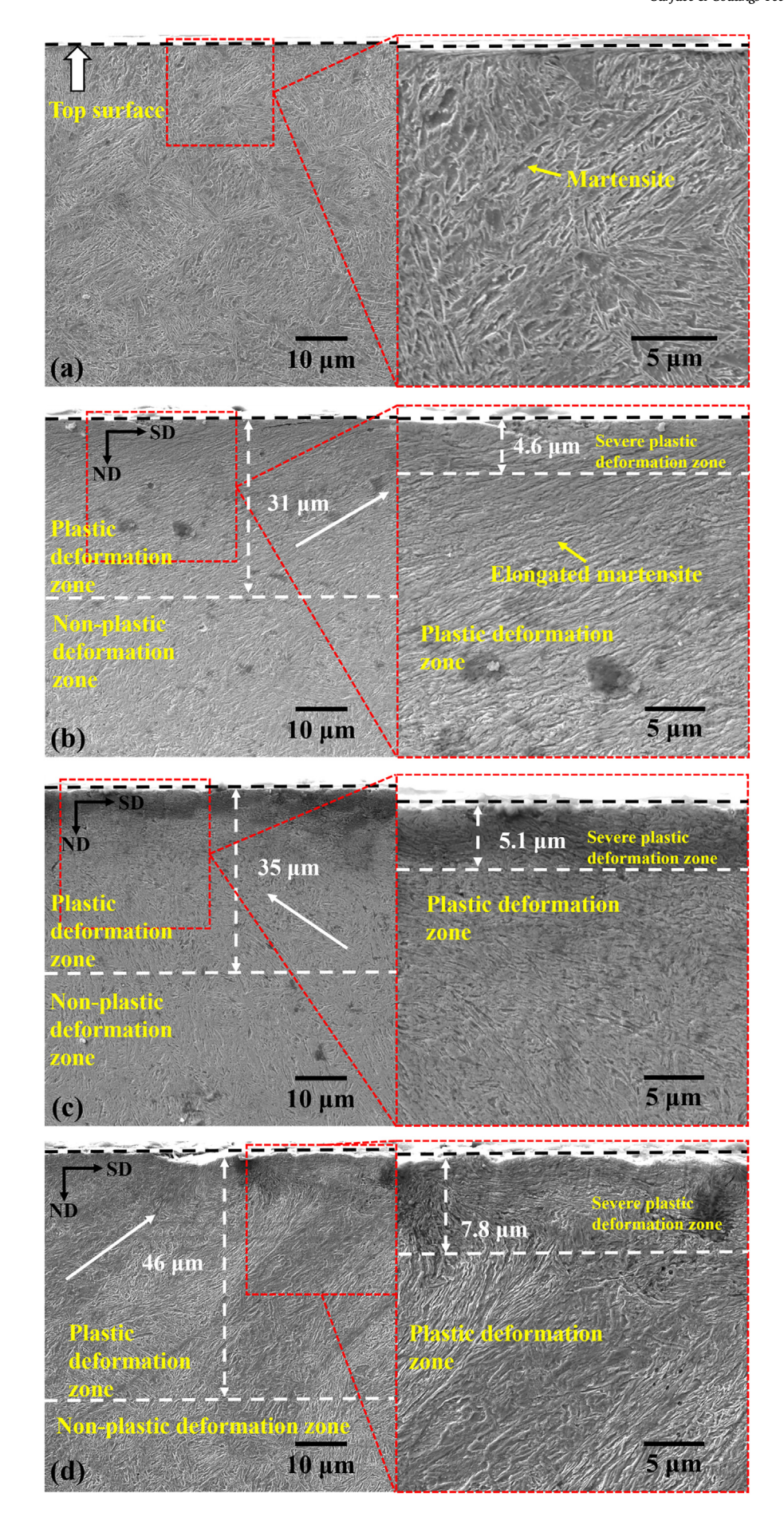


Fig. 4. SEM micrographs of cross-sectional microstructure for (a) control, (b) UNSM, (c) CC-UNSM and (d) EP-UNSM samples (SD = scanning direction, ND = normal direction).

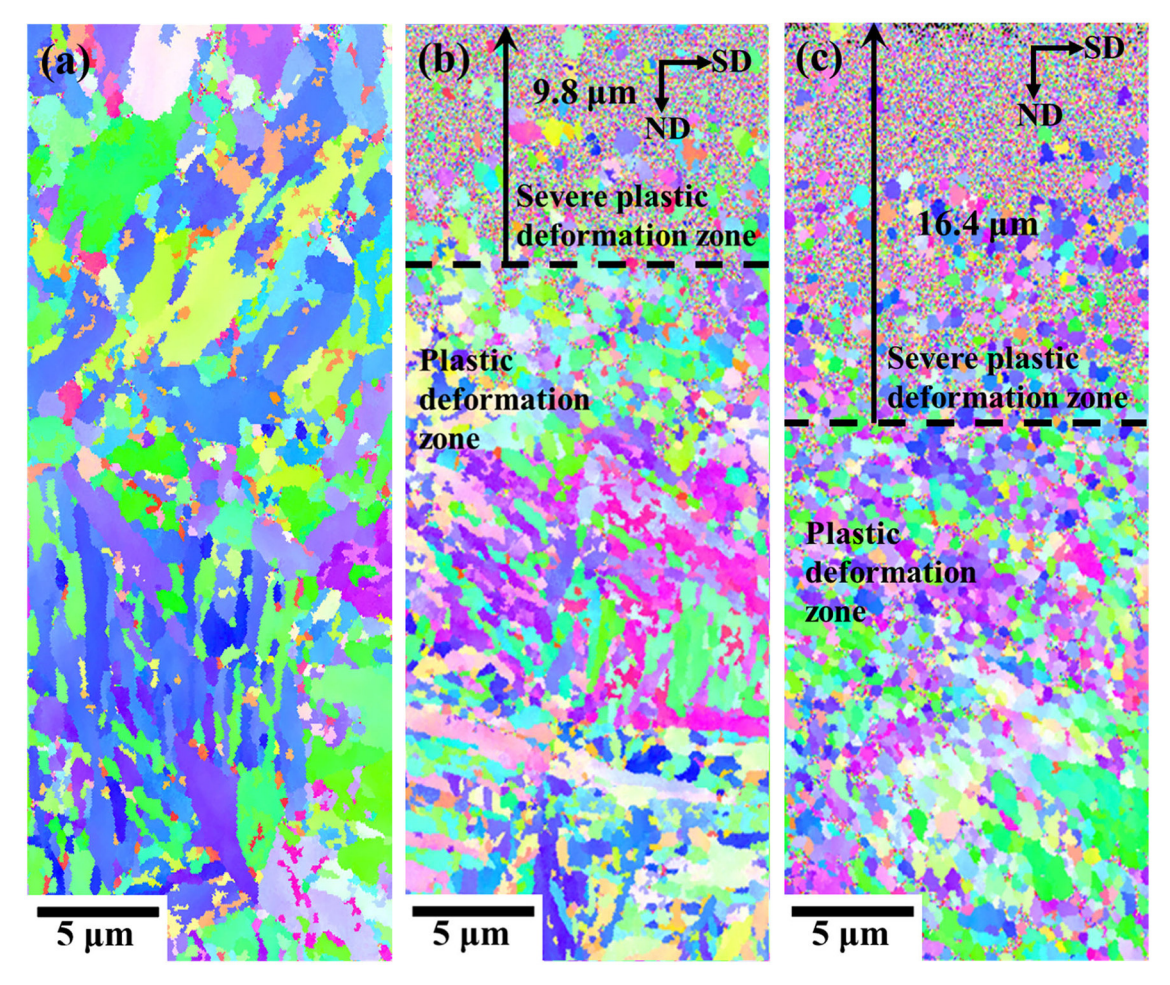


Fig. 5. EBSD micrographs showing the cross-sectional microstructure for the (a) control, (b) CC-UNSM and (c) EP-UNSM samples (SD = scanning direction, ND = normal direction).

2.2.3. Scanning electron microscopy

Scanning electron microscopy (SEM) was carried out in a Tescan Lyra 3 SEM system to observe the microstructure evolution of the samples. Prior to observation, all samples were polished using SiC sandpapers and a 1- μ m diamond suspension, followed by etching with a 4% Nital solution.

2.2.4. Electron backscatter diffraction

To characterize the microstructure of the samples, an electron backscatter diffraction (EBSD) study was carried out using a Genesis 4040 EBSD system in the Tescan Lyra 3 SEM using a scanning step size of 0.07 μ m and a scanning voltage of 20 kV. Prior to testing, all samples were mechanically polished using a 1- μ m diamond polishing suspension and 60-nm colloidal silica mixed with 10% hydrogen peroxide (H₂O₂).

2.2.5. Micro-hardness tests

To accurately measure the top surface hardness, all samples were lightly polished using SiC sandpaper and a 1- μ m diamond suspension. To measure the in-depth hardness, cross sections of the samples were polished using a 1- μ m diamond suspension. All hardness tests were performed on a Tukon 1202 Vickers hardness tester with a load of 50 g, where the holding time was 10 s.

2.2.6. Wear tests

The pin-on-disk (POD) test was conducted in a CSM Instruments tribometer using a load of 2 N and a frequency of 10 Hz. The wear test conditions were as follows: a tungsten carbide ball (Φ 6 mm) was used as the pin, the rotational speed was 10 cm/s, the wear distance was 300 m, and the wear radius was 3.5 mm. The wear tracks after wear testing were examined with the aid of a Zygo NewView 7300 surface profiler.

3. Results and discussion

3.1. Phase observation by XRD

Fig. 3a shows the XRD patterns of the control, UNSM, CC-UNSM and EP-UNSM samples. The XRD pattern of the control samples mainly contains three peaks: α (110), α (200) and α (211). This pattern shows that the main structure of 300M steel consists of martensite. After UNSM treatment, no new crystallization peaks appear in the XRD pattern. However, after CC-UNSM treatment, a new phase (Fe₂O₃) can be detected (Fig. 3b). Although the temperature and intensity of the new peaks are relatively low, the XRD pattern did indicate the existence of surface oxidation. Oxidation peaks can also be observed in the pattern for the EP-UNSM samples. However, due to the low temperature, the amount of oxide is small in both the CC-UNSM samples and the EP-

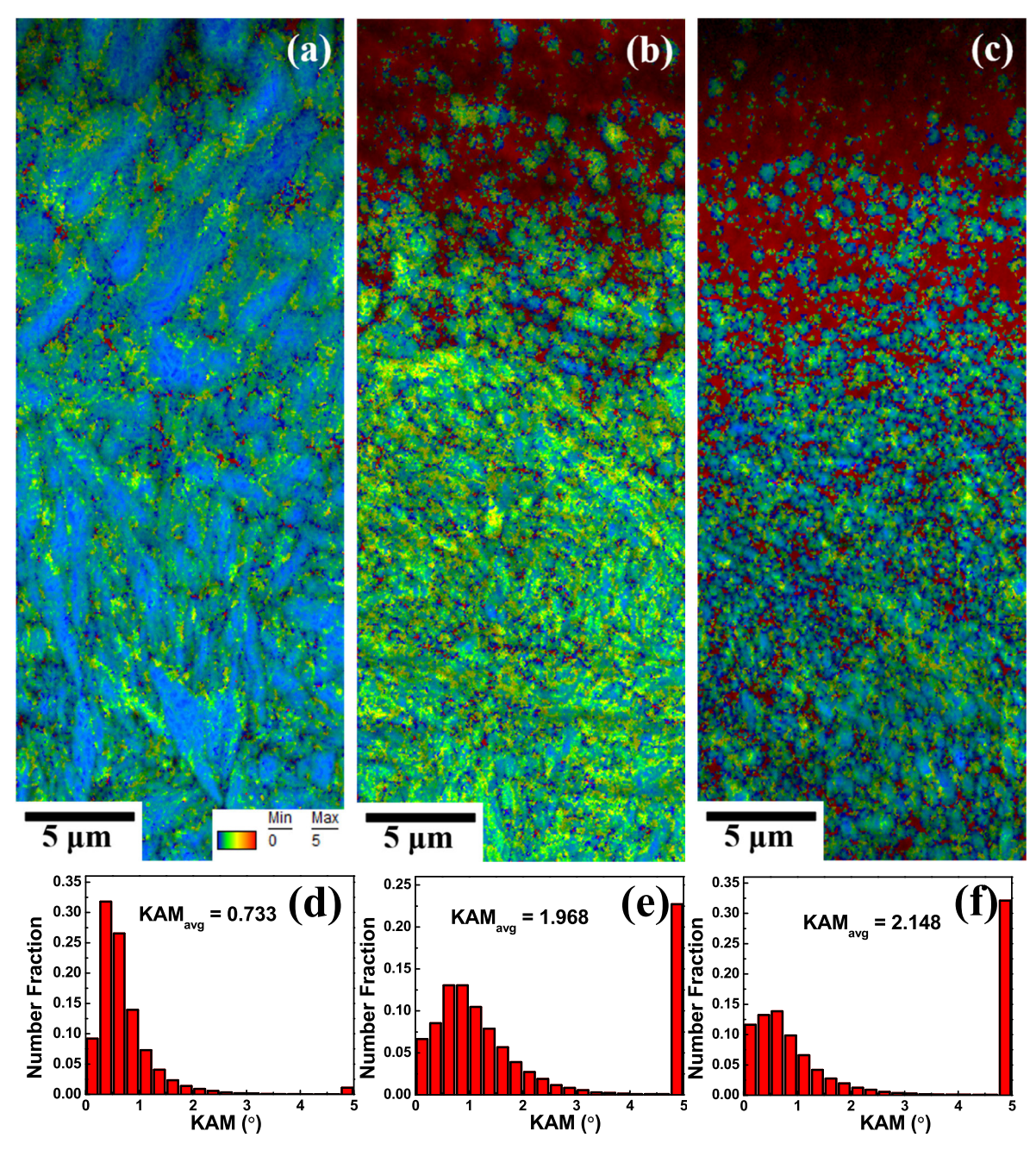


Fig. 6. KAM distribution maps and charts from cross sections of (a,d) control, (b,e) CC-UNSM and (c,f) EP-UNSM samples.

UNSM samples. In addition, as shown in Fig. 3c, the main α (110) peak of UNSM-treated samples has broadened, which reveals that the large plastic strain introduced by UNSM causes significant martensitic lath refinement and lattice distortion. Apparently, compared with samples treated using UNSM and CC-UNSM, the diffraction peak of α (110) for the EP-UNSM samples is not only wider but also shifts to a higher angle. This finding indicates that EP-UNSM processing might have resulted in more significant grain refinement; to determine if this has occurred, the results need to be confirmed using SEM and ESBD.

3.2. Cross-sectional microstructure observation by SEM

Fig. 4 exhibits the cross-sectional microstructure of the control 300M steel sample and the samples treated using UNSM, CC-UNSM and EP-UNSM. The main microstructure of the control samples consists of tempered martensite with different orientations (Fig. 4a). Because of

ultrasonic striking, a 31-µm surface plastic deformation (SPD) layer is found on the surface of the 300M steel following UNSM treatment (Fig. 4b). This deformation is particularly apparent in the region near the top surface of the sample, where the martensitic laths are severely refined, and the thickness of severe surface plastic deformation (SSPD) layer has increased to approximately 4.6 µm. In addition, the martensite laths in the SPD layer were found to lie parallel to the UNSM scanning direction. The depth of the SPD layer of the CC-UNSM sample has slightly increased to 35 μm (Fig. 4c). In addition, martensitic laths on the top surface are further refined, and the depth of the SSPD layer has increased to 5.1 µm. The reason for these improvements is that continuous current further enhances the plastic deformation capacity of the samples by increasing the sample temperature. The thickness of the SPD layer of the EP-UNSM samples has dramatically enhanced (to 46 μ m, as shown in Fig. 4d). In addition, the martensitic laths are dramatically refined and elongated, and the thickness of the SSPD layer

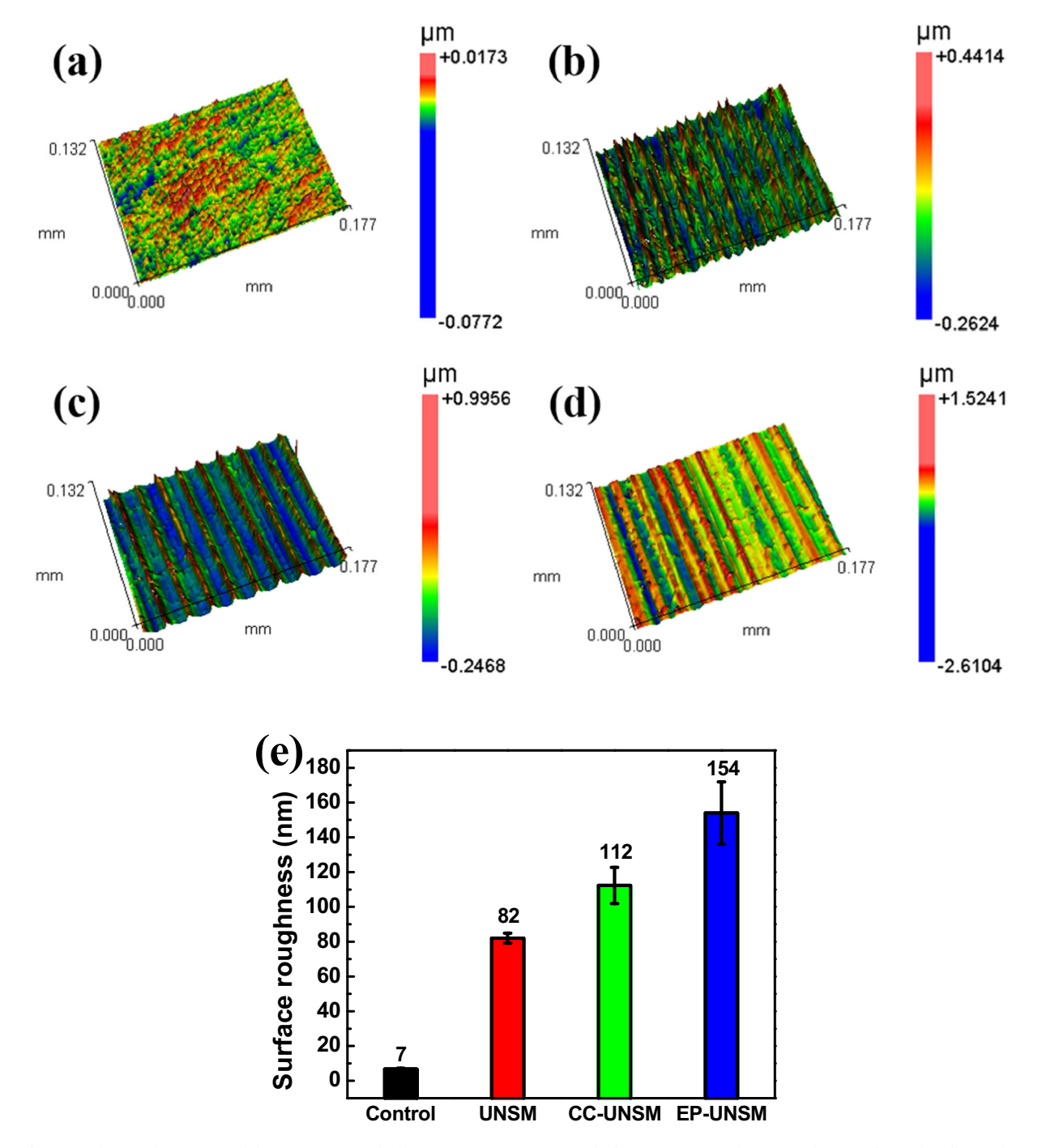


Fig. 7. Evolution of micromorphology in (a) control, (b) UNSM, (c) CC-UNSM, and (d) EP-UNSM samples; (e) surface roughness for all samples.

has increased to 7.8 $\mu m.$ This finding shows that even though the temperature for the two processes is the same, EP-UNSM treatment can produce deeper SPD and SSPD layers in the surface of the sample as compared to CC-UNSM treatment.

3.3. Cross-sectional microstructure observation by EBSD

To further compare the differences between CC-UNSM and EP-UNSM treatment, microstructural changes along the cross sections of the control, CC-UNSM and EP-UNSM samples were observed by EBSD as shown in Fig. 5. Compared with the control sample, the grain size of the CC-UNSM sample is significantly reduced. In the near-surface region, grains are so severely refined that the grain boundaries are difficult to distinguish. In addition, the depth of the severe surface plastic

deformation (SSPD) layer of the CC-UNSM sample can reach to 9.8 μm (Fig. 5b), which is thicker than that (5.1 μm) observed by SEM. The similar phenomenon has also been observed by Liu et al. [18], which is attributed to the fact that EBSD can provide more details about deformed grains than SEM. Similarly, EBSD shows that the EP-UNSM sample has an SSPD layer of 16.4 μm , compared with 7.8 μm observed by SEM. In addition, compared with that in the CC-UNSM sample, the grain refinement is more significant and the grain refinement region is deeper in the EP-UNSM sample.

Fig. 6 shows the kernel average misorientation (KAM) distribution for the treated and untreated samples. In the KAM images, the red and blue dots represent the degree of plastic deformation, with red indicating the highest amount of deformation and blue the lowest. As shown in Fig. 6a and d, very low misorientation and a small average

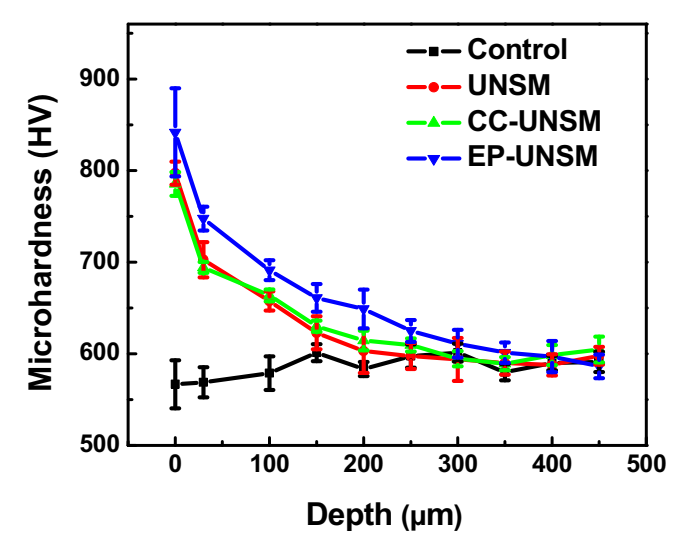
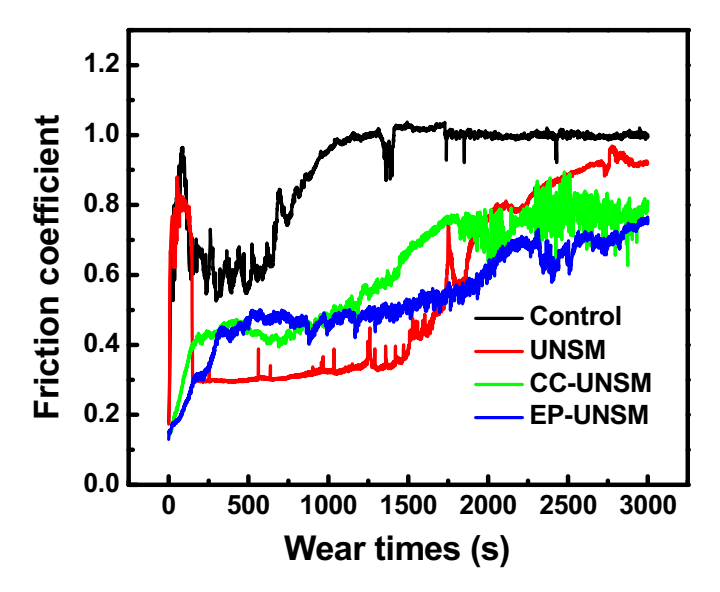


Fig. 8. In-depth hardness of the surfaces of control, UNSM, CC-UNSM, and EP-UNSM samples.



 ${\bf Fig.~9.}$ Friction coefficients of control, UNSM, CC-UNSM and EP-UNSM samples.

KAM value (0.733) can be observed in the control sample. After CC-UNSM treatment, high misorientation is observed near the top surface of the sample (Fig. 6b), and the average KAM value has also increased (1.968). This result reveals that CC-UNSM treatment has induced a larger plastic strain. After EP-UNSM treatment, higher misorientation and the largest average KAM value (2.148) were observed (Fig. 6c and f), indicating that EP can more effectively improve the plasticity of the 300M steel sample and thus lead to the highest plastic strain.

3.4. Surface morphology

Fig. 7 presents the surface topographies of the control, UNSM, CC-UNSM and EP-UNSM samples. While the surfaces of the control samples after mechanical polishing were very smooth, grooves were observed in the sample surface after UNSM treatment (Fig. 7b). Hence, UNSM treatment increased the surface roughness (from Ra = 7 nm to Ra = 82 nm). After CC-UNSM treatment, the surface roughness is further enhanced (to Ra = 112 nm), and deeper furrows are observed. EP-UNSM treatment resulted in the highest surface roughness, with an Ra value of 154 nm. The higher plasticity of the 300M steel samples

imparted by CC-UNSM and EP-UNSM treatment resulted in higher surface roughness. However, it should be noted that even though both CC-UNSM and EP-UNSM samples had higher surface roughness, the surface roughness is still at an acceptable level.

3.5. In-depth hardness

Fig. 8 shows the distribution of in-depth hardness of samples after being subjected to different treatments. It is observed that the top surface hardness of the control sample is 566.7 HV. After UNSM treatment, the top surface hardness is 797 HV. Due to the depth-gradient nature of the UNSM process, a gradient hardening layer of about 150 μm is induced. Work hardening and martensitic lath refinement are the major reasons for the higher hardness. CC-UNSM treatment resulted in a similar hardness distribution as compared to that for UNSM. In contrast, EP-UNSM treatment resulted in a much higher surface hardness (842 HV), which represents a 49% increase as compared to the control sample. In addition, the depth of the hardened layer of the EP-UNSM samples is 250 μm , which is much deeper than that of the UNSM samples (150 μm). Even though the temperature is very similar in CC-UNSM and EP-UNSM treatment, EP-UNSM treatment resulted in much higher surface hardness and a deeper hardened layer.

3.6. Wear resistance

Fig. 9 shows the friction coefficient of the control, UNSM, CC-UNSM, and EP-UNSM samples. Due to the high hardness of the grinding material, the control sample suffered serious wear damage. Hence, the friction coefficient of the control sample in the steady wear stage remains at 1.0. After UNSM treatment, the friction coefficient of the sample in the steady wear stage has reduced remarkably, to 0.3, as a result of the enhanced surface hardness. However, with the consumption of the surface hardened layer and the accumulation of abrasive debris, the friction coefficient gradually increased after 1500 s of wear damage. After CC-UNSM treatment, the sample has a higher surface hardness and also a higher surface roughness than the UNSM sample. As a result, the friction coefficient is slightly increased to 0.44. Although the EP-UNSM sample exhibits the highest values for surface hardness, it also has the highest surface roughness. As a result, the friction coefficient for the EP-UNSM sample (0.49) is very similar to that of the CC-UNSM sample.

Fig. 10a shows the wear rate of different samples after pin-on-disk (POD) testing under dry conditions. The average wear rate of the control samples is $6.2 \times 10^{-6} \text{ mm}^3 \text{ N}^{-1} \text{ m}^{-1}$. Due to the surface hardened layer in the UNSM samples, the average wear rate for these samples is significantly lower, at 3.9 \times 10⁻⁶ mm³ N⁻¹ m⁻¹. This finding suggests that UNSM treatment enhances the wear resistance of the sample. The CC-UNSM samples had an average wear rate of $3.7 \times 10^{-6} \text{ mm}^3 \text{ N}^{-1} \text{ m}^{-1}$, which was slightly lower than that for the UNSM samples. However, due to their much higher surface hardness, the EP-UNSM samples have the lowest average wear rate (3.4 \times 10⁻⁶ mm³ N⁻¹ m⁻¹). It is worth noting that compared with the CC-UNSM sample, the wear resistance of EP-UNSM has not been significantly improved. This is mainly because that the significantly increased surface roughness of the EP-UNSM treated sample enhances the contact pressure of the sample surface, which seriously hinders the further improvement of wear resistance. The profile measurements across the wear scars for all samples are exhibited in Fig. 10b. The tungsten carbide ball left a wear scratch with a depth of $0.6 \mu m$ on the surface of the control samples. Since a hardened layer is induced by UNSM treatment, the depth of wear scratch on the UNSM samples is significantly reduced to 0.38 µm. CC-UNSM treatment reduced this further, as the depth of the wear scratch in the CC-UNSM samples was $0.33 \mu m$. The EP-UNSM samples show the smallest depth of wear scratching (0.19 μ m).

As shown in Fig. 10c, a wear track with a width of $364~\mu m$ can be observed in the control sample. The width of the cracks in the UNSM,

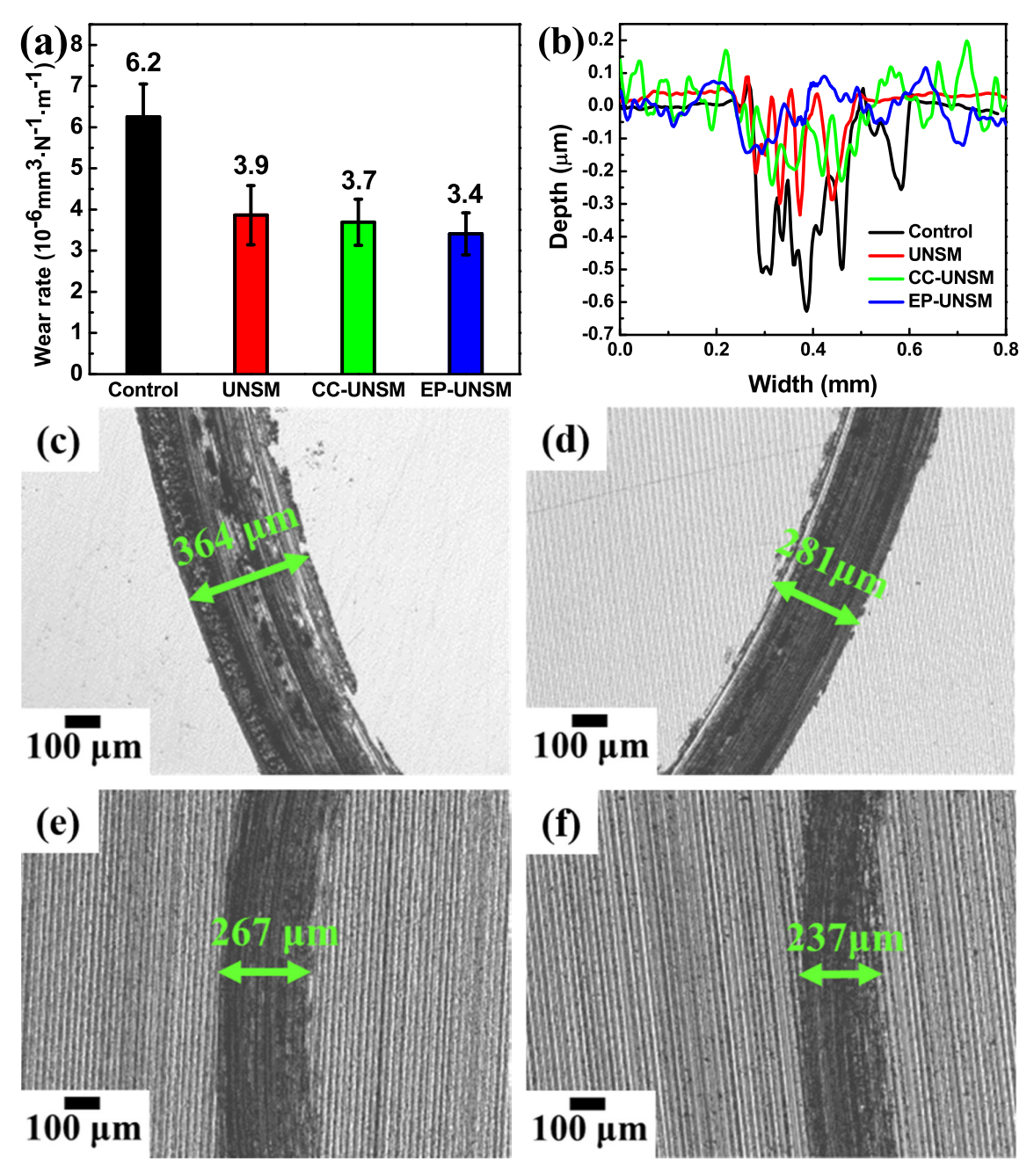


Fig. 10. Wear in the control, UNSM, CC-UNSM, and EP-UNSM samples: (a) wear rate after POD testing and (b) profile measurements across the wear scars. Zygo images of wear tracks for (c) control, (d) UNSM, (e) CC-UNSM, and (f) EP-UNSM samples.

CC-UNSM and EP-UNSM samples were 281 μm (Fig. 10d), 267 μm (Fig. 10e), and 237 μm (Fig. 10f), respectively. The three treatment processes showed a transition from severe wear to mild wear, with EP-UNSM treatment being the most effective. As was reported for control samples of 300M steel in our previous study [19], the main wear mechanisms of the 300M steel control samples in this study are abrasive wear and adhesive wear. All treated samples also have grooves and adhesions in the wear track, but the wear damage is dramatically reduced as compared to that of the control samples. Moreover, the wear mechanisms for the samples subjected to three different treatments are very similar.

4. Discussions

It is known that the processing effectiveness of UNSM depends on

the plasticity of the metal. To study whether EP can more effectively enhance the plasticity of 300M steel as compared to continuous current in the UNSM process, a single-line UNSM scan was carried out. In this test, the tip path was designed to leave only one line with a length of 7 mm on the sample surface, and the depth of the resulting scratch was measured. Each measurement of was repeated five times, and the average value was reported. In this test, a higher value for the scratch depth indicates a higher plasticity for the material. The micromorphology and depth of the scratches in all samples after single-line UNSM scans are presented in Fig. 11. The average scratch depth for the UNSM, CC-UNSM, and EP-UNSM samples are 2.78 μm , 2.9 μm and 3.26 μm , respectively. This implies that both continuous current and pulsed current can improve the plasticity of 300M steel and that the pulsed current is more effective, even though the temperature increase is the same.

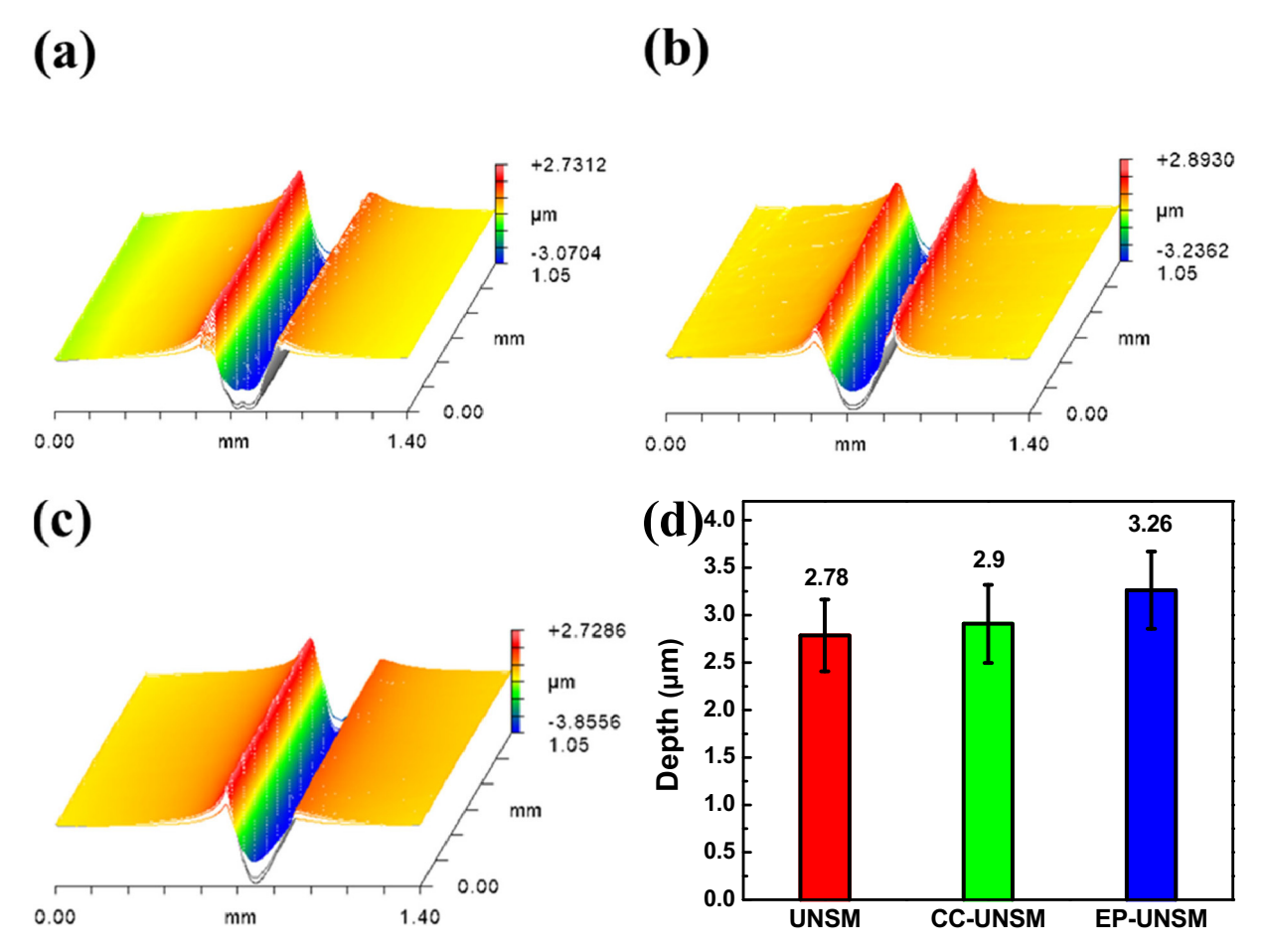


Fig. 11. Micromorphology of 300M steels treated using (a) UNSM, (b) CC-UNSM, and (c) EP-UNSM after a single-line UNSM scan. (d) Average scratch depth of UNSM, CC-UNSM and EP-UNSM samples after a single-line UNSM scan.

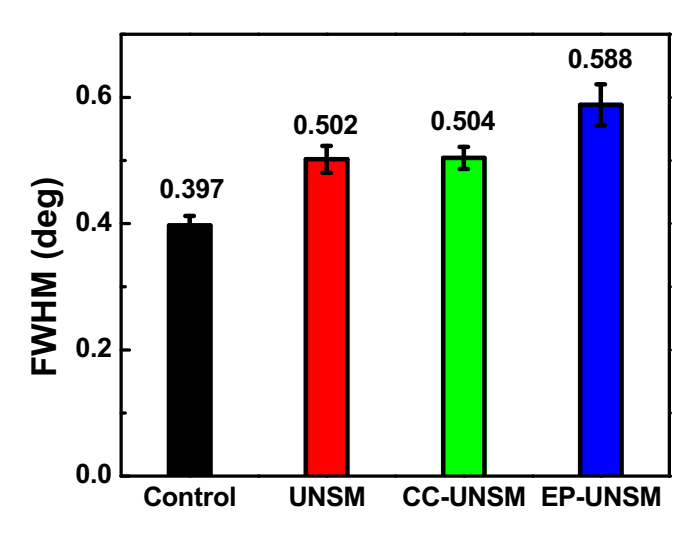


Fig. 12. FWHM values of the main α (110) plane reflections of control, UNSM, CC-UNSM, and EP-UNSM samples of 300M steels.

Since the UNSM process parameters are the same for UNSM, CC-UNSM and EP-UNSM, higher plasticity of the material would normally be expected to induce a greater amount of dislocation activity and thus higher dislocation density. Therefore, it is necessary to compare the dislocation densities of the treated samples. XRD is one of the most effective methods for measuring the relative dislocation density. Because the full width at half maximum (FWHM) value from the XRD peaks is directly proportional to the lattice defect density when the

grain size is similar, FWHM values of XRD peaks are commonly used to represent relative dislocation densities. Because the full width at half maximum (FWHM) value is directly proportional to the lattice defect density when the grain size is similar, FWHM values are commonly used to represent relative dislocation densities. The average FWHM values of the main α (110) XRD peak for the control, UNSM, CC-UNSM and EP-UNSM samples are 0.397, 0.502, 0.504 and 0.588, respectively (Fig. 12). These results imply that the dislocation densities of the samples rapidly increased due to UNSM treatment. However, for samples treated using CC-UNSM, the average FWHM value is very similar to that for samples treated by UNSM alone; this finding shows that the thermal effect induced by continuous current at such a low temperature (below 150 °C) cannot significantly promote dislocation motion in 300M steel. Compared to that for the CC-UNSM treatment, the FWHM value for EP-UNSM treated samples is significantly higher, with an average of 0.588. This finding demonstrates that pulsed current is much more effective compared with continuous current in energizing dislocation movement—even though the temperature is the same.

A schematic representation of the deformation mechanisms for UNSM, CC-UNSM, and EP-UNSM is presented in Fig. 13. During UNSM treatment, ultrasonic striking introduces plastic strain on the surface of the 300M steel. As a result, dislocation accumulation, rearrangement, and annihilation occurred in the near-surface region of the samples. With the increase in plastic strain, dislocations interact to form dislocation walls (DWs) and dislocation tangles (DTs). The DWs and DTs gradually evolve into sub-boundaries to minimize system energy. In addition, some twins are also triggered in the stress concentration zone due to strain hardening. Finally, the sub-grain boundaries gradually evolve into grain boundaries, which increases surface grain refinement.

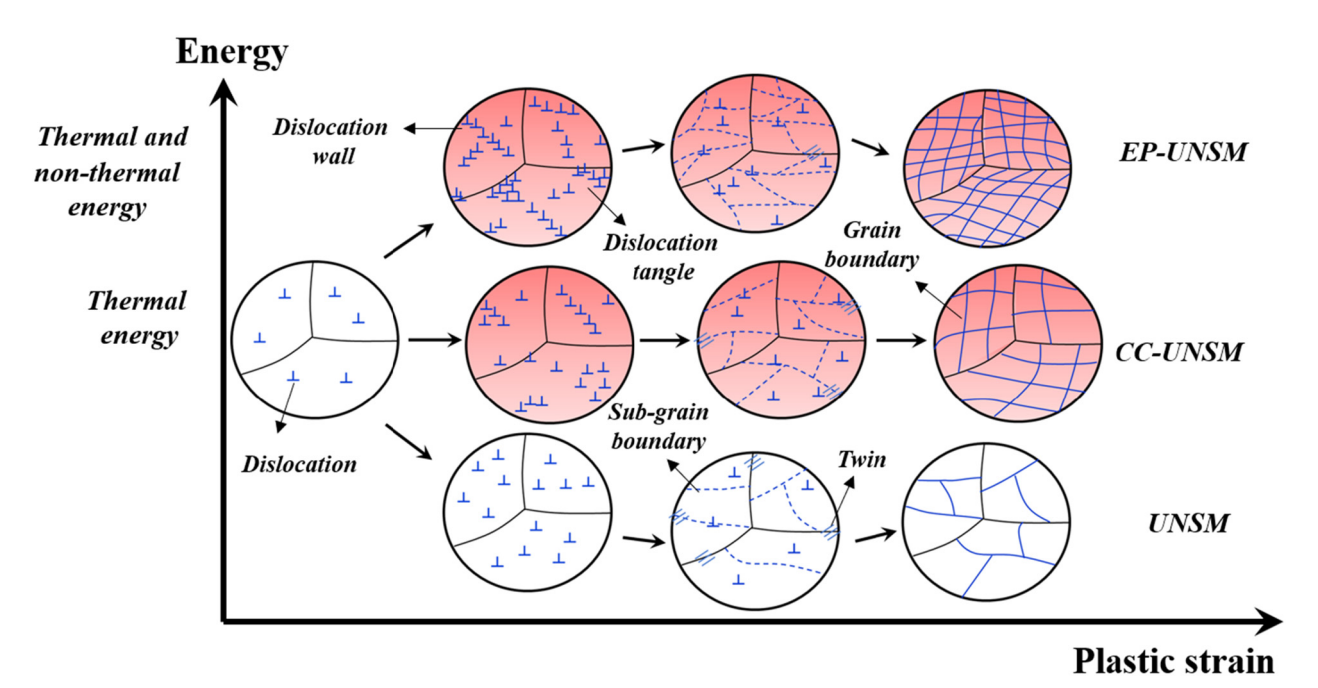


Fig. 13. Deformation mechanisms of 300M steel treated by UNSM, CC-UNSM, and EP-UNSM.

Because continuous current can induce thermal softening [20,21], the generation and migration rates of dislocations increase. As a result, more DTs and DWs are found in the grains of the CC-UNSM samples as compared to UNSM samples. Hence, the surface grains are further refined, and deeper and larger plastic deformation layers are generated in the surfaces of the CC-UNSM samples.

In contrast, a pulsed current is more effective for enhancing the plasticity of 300M steel. It is believed that pulsed current, due to a much higher peak current density than a continuous current with the same effective current density, can more effectively mobilize pinned dislocations and thus promote dislocation motion during EP-UNSM. Dislocations that are more mobile are able to generate more DWs and DTs and, thus, produce more significant grain refinement. Hence, as compared to UNSM and CC-UNSM treatments, EP-UNSM treatment produced the most significant grain refinement, which lead to much higher surface hardness and plastically affected depth.

5. Conclusions

In this study, combinations of UNSM with pulsed current and continuous current were used to treat 300M steel. The use of a pulsed current resulted in more energized dislocation movement during EP-UNSM treatment, thereby leading to more significant grain refinement and a much higher dislocation density. Compared with CC-UNSM treatment, EP-UNSM treatment resulted in a plastic deformation layer that is 31% deeper and a much higher surface hardness, even though the bulk temperature for the samples in both processes is the same. This result indicates that the beneficial effects induced by EP-UNSM treatment cannot be fully explained by the thermal effect. Due to their much higher surface hardness, EP-UNSM samples have a much higher wear resistance than those of the control, UNSM and CC-UNSM samples. This study demonstrates that EP-UNSM is a promising method for improving the surface strength and mechanical properties of difficult-to-deform materials without the need to increase the processing temperature significantly.

CRediT authorship contribution statement

Weidong Zhao: Investigation, Data curation, Writing - original draft. Daoxin Liu: Supervision, Funding acquisition. Xiaohua

Zhang: Investigation. Hao Zhang: Investigation. Jun Liu: Investigation, Data curation. Chi Ma: Formal analysis, Data curation. Ruixia Zhang: Data curation, Writing - review & editing. Yalin Dong: Resources, Writing - review & editing, Supervision. Chang Ye: Conceptualization, Writing - review & editing, Funding acquisition.

Declaration of competing interest

The authors declare no conflict of interest.

Acknowledgments

W. Zhao, D. Liu and X. Zhang would like to acknowledge the support of this work by the National Natural Science Foundation of China (grant no. 51771155) and the China Scholarship Council. H. Zhang, J. Liu, C. Ma, R. Zhang, Y. Dong and C. Ye would like to acknowledge the financial support of this work by the National Science Foundation CAREER program (grant no. CMMI 1847247).

References

- A. Gill, A. Telang, S.R. Mannava, D. Qian, Y.S. Pyoun, H. Soyama, V.K. Vasudevan, Comparison of mechanisms of advanced mechanical surface treatments in nickelbased superalloy, Mater. Sci. Eng. A 576 (2013) 346–355, https://doi.org/10.1016/ j.msea.2013.04.021.
- [2] A. Amanov, P. Oleksiy V, P. Young-Sik, D.-E. Kim, Effects of ultrasonic nanocrystalline surface modification on the tribological properties of AZ91D magnesium alloy, Tribol. Int. 54 (2012) 106–113, https://doi.org/10.1016/j.triboint.2012.04.024.
- [3] C. Ye, A. Telang, A.S. Gill, S. Suslov, Y. Idell, K. Zweiacker, J.M.K. Wiezorek, Z. Zhou, D. Qian, S.R. Mannava, V.K. Vasudevan, Gradient nanostructure and residual stresses induced by ultrasonic nano-crystal surface modification in 304 austenitic stainless steel for high strength and high ductility, Mater. Sci. Eng. A 613 (2014) 274–288, https://doi.org/10.1016/j.msea.2014.06.114.
- [4] C. Ye, X. Zhou, A. Telang, H. Gao, Z. Ren, H. Qin, S. Suslov, A.S. Gill, S.R. Mannava, D. Qian, G.L. Doll, A. Martini, N. Sahai, V.K. Vasudevan, Surface amorphization of NiTi alloy induced by ultrasonic nanocrystal surface modification for improved mechanical properties, J. Mech. Behav. Biomed. Mater. 53 (2016) 455–462, https://doi.org/10.1016/j.jmbbm.2015.09.005.
- [5] B. Wu, J. Zhang, L. Zhang, Y.S. Pyoun, R.I. Murakami, Effect of ultrasonic nanocrystal surface modification on surface and fatigue properties of quenching and tempering S45C steel, Appl. Surf. Sci. 321 (2014) 318–330, https://doi.org/10. 1016/j.apsusc.2014.09.068.
- [6] A. Amanov, I.-S. Cho, Y.-S. Pyun, Microstructural evolution and surface properties

- of nanostructured Cu-based alloy by ultrasonic nanocrystalline surface modification technique, Appl. Surf. Sci. 388 (2016) 185–195, https://doi.org/10.1016/j.apsusc. 2016.01.237.
- [7] Z. Zhao, S. To, Z. Sun, R. Ji, K.M. Yu, Microstructural effects of Ti6Al4V alloys modified by electropulsing treatment on ultraprecision diamond turning, J. Manuf. Process. 39 (2019) 58–68, https://doi.org/10.1016/j.jmapro.2019.02.005.
- [8] A.J. Sánchez Egea, H.A. González Rojas, C.A. Montilla Montaña, V. Kallewaard Echeverri, Effect of electroplastic cutting on the manufacturing process and surface properties, J. Mater. Process. Technol. 222 (2015) 327–334, https://doi.org/10. 1016/j.jmatprotec.2015.03.018.
- [9] S. Hameed, H.A. González, R. Id, J.I.P. Benavides, Influence of the regime of electropulsing-assisted machining on the plastic deformation of the layer being cut, Materials (Basel) 11 (2018) 1–10, https://doi.org/10.3390/ma11060886.
- [10] Y. Ye, S.Z. Kure-Chu, Z. Sun, X. Li, H. Wang, G. Tang, Nanocrystallization and enhanced surface mechanical properties of commercial pure titanium by electropulsing-assisted ultrasonic surface rolling, Mater. Des. 149 (2018) 214–227, https://doi.org/10.1016/j.matdes.2018.04.027.
- [11] H. Wang, G. Song, G. Tang, Evolution of surface mechanical properties and microstructure of Ti-6Al-4V alloy induced by electropulsing-assisted ultrasonic surface rolling process, J. Alloys Compd. 681 (2016) 146–156, https://doi.org/10.1016/j. iallcom.2016.04.067.
- [12] R. Ji, Z. Yang, H. Jin, Y. Liu, H. Wang, Q. Zheng, W. Cheng, B. Cai, X. Li, Surface nanocrystallization and enhanced surface mechanical properties of nickel-based superalloy by coupled electric pulse and ultrasonic treatment, Surf. Coat. Technol. 375 (2019) 292–302, https://doi.org/10.1016/j.surfcoat.2019.07.037.
- [13] H. Zhang, Z. Ren, J. Liu, J. Zhao, Z. Liu, D. Lin, R. Zhang, M.J. Graber, N.K. Thomas, Z.D. Kerek, G.X. Wang, Y. Dong, C. Ye, Microstructure evolution and electroplasticity in Ti64 subjected to electropulsing-assisted laser shock peening, J. Alloys Compd. 802 (2019) 573–582, https://doi.org/10.1016/j.jallcom.2019.06.156.

- [14] R. Ji, Y. Liu, S. To, H. Jin, W. Sze, Z. Yang, Efficient fabrication of gradient nanostructure layer on surface of commercial pure copper by coupling electric pulse and ultrasonics treatment, J. Alloys Compd. 764 (2018) 51–61, https://doi.org/10. 1016/j.jallcom.2018.06.042.
- [15] J. Zhao, Z. Ren, H. Zhang, G.X. Wang, Y. Dong, C. Ye, Electroplasticity in AZ31B subjected to short-duration high-frequency pulsed current, J. Appl. Phys. 125 (2019) 185104, https://doi.org/10.1063/1.5087465.
- [16] C. Ma, S. Suslov, C. Ye, Y. Dong, Improving plasticity of metallic glass by electropulsing-assisted surface severe plastic deformation, Mater. Des. 165 (2019) 107581, https://doi.org/10.1016/j.matdes.2019.107581.
- [17] Yongda Ye, Haibo Wang, Guoyi Tang, Guolin Song, Effect of electropulsing-assisted ultrasonic nanocrystalline surface modification on the surface mechanical properties and microstructure of Ti-6Al-4V alloy, J. Mater. Eng. Perform. 27 (2018) 2394–2403, https://doi.org/10.1007/s11665-018-3248-3.
- [18] C. Liu, D. Liu, X. Zhang, S. Yu, W. Zhao, Effect of the ultrasonic surface rolling process on the fretting fatigue behavior of Ti-6Al-4V alloy, Materials (Basel) 10 (2017) 833, https://doi.org/10.3390/ma10070833.
- [19] W. Zhao, D. Liu, H. Qin, X. Zhang, H. Zhang, R. Zhang, Z. Ren, C. Ma, A. Amanov, Y.-S. Pyun, G.L. Doll, Y. Dong, C. Ye, The effect of ultrasonic nanocrystal surface modification on low temperature nitriding of ultra-high strength steel, Surf. Coat. Technol. 375 (2019) 205–214, https://doi.org/10.1016/j.surfcoat.2019.07.006.
- [20] H. Zhang, J. Zhao, J. Liu, H. Qin, Z. Ren, G.L. Doll, Y. Dong, C. Ye, The effects of electrically-assisted ultrasonic nanocrystal surface modification on 3D-printed Ti-6Al-4V alloy, Addit. Manuf. 22 (2018) 60–68, https://doi.org/10.1016/j.addma. 2018.04.035.
- [21] J. Liu, S. Suslov, S. Li, H. Qin, Z. Ren, G.L. Doll, H. Cong, Y. Dong, C. Ye, Electrically assisted ultrasonic nanocrystal surface modification of Ti6Al4V alloy, Adv. Eng. Mater. 20 (2018) 1700470, https://doi.org/10.1002/adem.201700470.